Biomedical nanoparticles modulate specific CD4$^+$ T cell stimulation by inhibition of antigen processing in dendritic cells

FABIAN BLANK[1], PETER GERBER[1], BARBARA ROTHEN-RUTISHAUSER[2], USAWADEE SAKULKHU[3], JATUPORN SALAKLANG[3,5], KARIN DE PEYER[1], PETER GEHR[2], LAURENT P. NICOD[4], HEINRICH HOFMANN[3], THOMAS GEISER[1], ALKE PETRI-FINK[3,5]*, & CHRISTOPHE VON GARNIER1*

[1]*Department of Clinical Research, Division of Pulmonology, Bern University Hospital, Bern, Switzerland,* [2]*Institute of Anatomy, Division of Histology, University of Bern, Bern, Switzerland,* [3]*Powder Technology Laboratory, École Polytechnique Fédérale de Lausanne, Lausanne, Switzerland,* [4]*Division of Pulmonology, Lausanne University Hospital, Lausanne, Switzerland, and* [5]*Department of Chemistry, University of Fribourg, Fribourg, Switzerland*

Abstract

Understanding how nanoparticles may affect immune responses is an essential prerequisite to developing novel clinical applications. To investigate nanoparticle-dependent outcomes on immune responses, dendritic cells (DCs) were treated with model biomedical poly(vinylalcohol)-coated super-paramagnetic iron oxide nanoparticles (PVA-SPIONs). PVA-SPIONs uptake by human monocyte-derived DCs (MDDCs) was analyzed by flow cytometry (FACS) and advanced imaging techniques. Viability, activation, function, and stimulatory capacity of MDDCs were assessed by FACS and an *in vitro* CD4$^+$ T cell assay. PVA-SPION uptake was dose-dependent, decreased by lipopolysaccharide (LPS)-induced MDDC maturation at higher particle concentrations, and was inhibited by cytochalasin D pre-treatment. PVA-SPIONs did not alter surface marker expression (CD80, CD83, CD86, myeloid/plasmacytoid DC markers) or antigen-uptake, but decreased the capacity of MDDCs to process antigen, stimulate CD4$^+$ T cells, and induce cytokines. The decreased antigen processing and CD4$^+$ T cell stimulation capability of MDDCs following PVA-SPION treatment suggests that MDDCs may revert to a more functionally immature state following particle exposure.

Keywords: *SPIONs, dendritic cells, immune response, antigen processing, antigen presentation*

Introduction

The development of novel nanotechnology-based pharmaceutical compounds has been constantly increasing over recent years, with some products already approved for clinical use. Although more than 200 biomedical nanomaterials were estimated to be under development in the year 2006 (defined as a material that has one or more external dimensions in the nanoscale) no guidelines exist to date that specifically regulate synthesis and testing of these products, for human use (Powers 2006; International Organization for Standardization [ISO] 2008). Recently, both European and US regulatory agencies have provided recommendations to address utilization of nanotechnology-based biomedical products in humans (European Medicines Agency [EMEA] 2006; U.S. Food and Drug Administration [FDA] 2007).

Super-paramagnetic iron-oxide nanoparticles (SPIONs) represent a versatile and multi-functional class of promising biomedical nanoparticles that combine advantageous properties of an inorganic metal core with specifically designed functionality of a biocompatible polymer shell (Boyer et al. 2010). The particle surface confers outstanding properties to SPIONs and nanoparticles in general, including stabilization in biological fluids (colloids), or specific cell targeting to enhance drug or gene delivery. These unique physico-chemical properties, together with super-paramagnetism, provide many useful advantages for existing diagnostic clinical areas such as magnetic

Correspondence: Dr Christophe von Garnier, Pulmonary Medicine, Inselspital, Bern University Hospital, Freiburgstrasse, Bern, Switzerland. Tel: +41 31632 2111. Fax: +41 31632 9833. E-mail: christophe.vongarnier@insel.ch
*APF and CVG contributed equally to this paper.

resonance imaging (MRI), as well as for novel biomedical approaches with therapeutic drug or gene delivery, tissue engineering, and bio-separation (Laurent et al. 2008).

One of the major difficulties in the development of appropriate biomedical nanoparticles for specific clinical applications is our current deficit in the understanding of how nanoparticles may influence immune responses (Dobrovolskaia and McNeil 2007; Dobrovolskaia et al. 2009). Despite an important body of epidemiological and experimental research on ambient particulate matter and engineered nanoparticles that has addressed conventional toxicological aspects, it is not possible at present to predict immune and inflammatory responses a specific type and size of nanoparticle may trigger (Oberdörster et al. 2005; Maynard et al. 2006; Dobrovolskaia and McNeil 2007). Several factors lie behind this lack of knowledge: With few exceptions, physico-chemical properties of nanoparticles (e.g. surface charge), their shell characteristics (polymer type), and behaviour in different colloidal solutions have not been systematically characterized to date, especially with respect to interaction with immune cells (Foged et al. 2005; Dobrovolskaia and McNeil 2007). Furthermore, for the synthesis of nanoparticles destined for biomedical applications, a great deal of differences in the raw materials employed and lack of standardized manufacturing processes have rendered comparison between nanoparticles from different research groups problematical.

The immunological properties of nanoparticles may be broadly determined by characteristics related to antigenicity, adjuvant behaviour, generation of inflammatory mediators, predominant internalization pathway(s), and immune cell type(s) most likely encountered (Chen et al. 1998; Dobrovolskaia and McNeil 2007; Manolova et al. 2008; Klippstein and Pozo 2010). In general, nanoscale drugs and diagnostic compounds are either being specifically designed for immunomodulation through their interaction with the immune system (e.g. nano-vaccines), or these formulations are specifically engineered to evade recognition by the immune system. For both situations, clarifying how nanoscale compounds interact with the immune system is crucial in order to understand which key characteristics of these compounds determine immune responses and to improve their design for future therapeutic or diagnostic applications (Dobrovolskaia and McNeil 2007; Dobrovolskaia et al. 2008, 2009).

The administration of drugs via mucosal surfaces (i.e. respiratory or gastro-intestinal tract) is attractive for reasons such as accessibility, needle-free administration, and site-specific action. Epithelia at the interfaces between the organism and environment are endowed with antigen-presenting cells (APC) that constantly scrutinize incoming antigen. Therefore, for the development of appropriate nanoscale compounds delivered to mucosal environments, their interaction with most frequently encountered APC, including DCs, macrophages and B cells, requires careful clarification. DCs are known to be the most specialized APC type, capable of presenting antigen to naïve T cells in the lymph nodes through cognate interactions, and thus are fundamental in orchestrating both innate and adaptive immune responses. DCs are primarily localized near the interfaces between body surfaces and the environment, where they continuously assess incoming antigen and particulate matter for the potential danger they may represent for the organism (Holt and Stumbles 2000). For example, the large mucosal surface area of the respiratory tract is continuously exposed to large amounts of antigen and particulate matter, and DCs form a tightly enmeshed mucosal network localized in the epithelium of conducting airways and lung parenchyma. This localization enables continuous scrutiny of inhaled antigen or particulates, either inducing tolerance to inoffensive substances, or initiating immunity against allergens or potentially harmful pathogens (von Garnier et al. 2005). A prerequisite for immunological homeostasis at this site are stringent control mechanisms to protect the vital and exquisitely fragile gaseous exchange barriers from damage that an exaggerated immune response to an innocuous allergen may cause (von Garnier and Nicod 2009). During DC activation, there is up-regulation of co-stimulatory molecules, maturation markers, and chemokine receptor CCR7 that enables DC migration to regional lymph nodes for activation of naïve T cells. DC activation is also accompanied by chemokine and cytokine release that not only serves to amplify innate immune responses, but also determines the type of effector T cell population and net immune response generated. Given the importance of DCs as sentinel cells in regulating innate and adaptive immune functions, studying functional changes that DCs may undergo when exposed to nanoscale compounds is central to understanding the impact on subsequent mucosal immune responses. We herein report our results obtained from a robust *in vitro* pre-clinical monocyte-derived human DCs (MDDCs) model that was utilized to assess immune effects of prototypical biomedical SPIONs. Studies were performed on immature MDDCs or on MDDCs cultured in the presence of lipopolysaccharide (LPS) to mature the cells and simulate inflammatory changes in the microenvironment. The findings obtained with this approach may

have important implications when designing specific immunomodulatory properties of novel biomedical nanoparticles.

Materials and methods

Nanoparticle synthesis, labelling, and characterization

Reagents. All reagents were of analytical reagent grade and utilized without further purification. Polyvinyl alcohol PVA (Mowiol 3–85), with an average molecular weight (MW) of 14,000 g/mol and a hydrolysis degree of 85%, was supplied by courtesy of KURARAY (Kuraray Specialties Europe GmbH, 65926 Frankfurt/ Main, Germany). Vinyl alcohol/ vinyl amine copolymer M12, with an average MW of 80,000–140,000, was supplied by courtesy of SEKISUI (Sekisui Specialty Chemicals Europe, 43080 Tarragona, Spain). Polymer solutions were prepared by dissolving the powders in water followed by rapidly heating and subsequent filtration of the hot solutions over paper filters (Schleicher & Schuell AG). Ultrapure deionized water (Seralpur delta UV/UF setting, 0.055 S/cm) was used in all synthesis steps. D-9527 Sigma cellulose membrane dialysis tubing with a molecular weight cut-off at 12,000 was used for dialysis.

Particle size. Light scattering measurements were performed at 90° on a photon correlation spectrometer (PCS) from Brookhaven equipped with a BI-9000AT digital auto-correlator. The CONTIN method was used for data processing. The concentration of iron oxide nanoparticles was set to 100 μg iron/ml for all measurements. The theoretical refractive index of 2.42 of magnetite was used to calculate the number weighted distribution from the raw intensity weighted data. Zeta-potential measurements were performed using the same setting, equipped with a platinum electrode. The electrode was cleaned for 10 min in an ultrasonic bath prior to each measurement and pre-equilibrated for 2 min in an aliquot of the sample. Viscosity, refractive index, and dielectric constant of pure water were used to characterise the solvent.

Superparamagnetic iron oxide nanoparticles (SPIONs). Nanoparticle synthesis and characterization were performed as previously described (Petri-Fink and Hofmann 2007). Briefly, SPIONs were prepared by alkaline co-precipitation of ferric and ferrous chlorides in aqueous solution (Bee et al. 1995; Chastellain et al. 2004). The obtained precipitate was washed several times with ultrapure water and the remaining solid was refluxed in nitric acid (10 M) in the presence of Iron-(III)-nitrate (FLUKA). The resulting suspension was dialysed against 0.01 M nitric acid (FLUKA) for two days, and stored at 4°C.

Polymer-coated particles. Polymer-coated SPIONs were produced as described elsewhere (Petri-Fink et al. 2005). Magnetic nanoparticles were stabilized by a mixture of polyvinyl alcohol (Mowiol 3–85) and vinyl alcohol/vinyl amine copolymer (M12, vinyl alcohol/vinyl alcohol copolymer mass ratio). The product will be referred to as PVA-SPION. The iron content of the suspension was determined by redoxtitration. In order to quantify the amount of surface adsorbed polymer, a colorimetric assay was developed based on the polyvinyl alcohol-iodine-boric acid complex (Baumgartner 1987). The assay was carried out in a 96-well plate and absorbance of yellow-green complexes was read at 668 nm by a TECAN plate reader (TECAN, Infinite).

Fluorochrome coupling and SPION characterization. Surface derivatization of PVA-coated SPIONs was performed in the previously described magnetic bed reactor (Steitz et al. 2007). Briefly, PVA-SPIONs were loaded and immobilized in the reactor. Dye coupling was achieved by re-circulating 250 μg Oregon green (Oregon green protein labelling kit (F6153), Invitrogen) or 100 μg Alexa 680 (Alexa 680 carboxylic acid, succinimidyl ester (A20008), Invitrogen), respectively, in 0.1 M carbonate buffer (pH 9.5) over immobilized nanoparticles for 2–4 h with a flow rate of 2.5 ml/min. After the reaction, free dye was removed before re-circulating 0.1 M lysine in 0.1 M carbonate buffer (pH 9.5) for 1 h at a flow rate of 2.5 ml/min. Excess lysine was removed by extensive washing with PBS (pH 7.4). In a final step, functionalized particles were eluted from the magnetic reactor and extensively characterized before and after dye coupling (Table I). Following dye coupling, the iron

Table I. Summary of particle properties before and after dye coupling.

Parameters	PVA-SPIONs	OG-PVA-SPIONs	Alexa-PVA-SPIONs
Iron conc. [mg/ml]	4.4	1	1
PVA conc. [mg/ml]	22.1	4.5	7.9
Dye conc. [μg/ml]	-	1.5	8.6
Dye molecules/particle	-	~40	~6
Size [nm]	29.4 ± 4.1	122.1 ± 14.6	117.0 ± 8.17
Zeta potential [mV]	+16.7 ± 1.5	+6.7 ± 2.2	+5.6 ± 1.2
pH	7.2	7.4	7.3
Particles/μl [$\times 10^{10}$]	9	2	2

OG, Oregon green; Alexa, Alexa Fluor 680.

concentration was set to 1 mg/ml by dilution in PBS. After dye coupling, the polymer/iron ratio was slightly decreased, most likely due to extensive purification of final particles in the reactor leading to loss of surface stabilizing macromolecules (i.e. PVA) that causes a relatively important increase in particle size (Table I).

Although the augmented particle size is mainly attributable to the presence of dye molecules, a certain degree of agglomeration within the final preparation cannot be entirely excluded. Nevertheless, the PVA-SPIONs utilized for all subsequent investigations were highly colloidally stable in all solutions (e.g. cell culture media) and environments tested (Petri-Fink and Hofmann 2007). The zeta potential (surface charge) decreased from +16.7 mV to +6.7 mV, indicating significant coupling of both Oregon green and Alexa Fluor 680 fluorochromes to amine groups of the polymer coating. The zeta potential of derived particles remained slightly positive, which was proven to be very helpful to enable cellular internalization in previous studies (Petri-Fink et al. 2005). Combination of a specifically designed polymer coating for SPIONs (e.g. PVA) with a fluorescence label therefore provided nanoparticles with both a "tracking signal" (fluorescence signal and electron-dense iron oxide core) and a potential affinity for targeted cell types (MDDCs). Labelled PVA-SPIONs destined for *in vitro* cell experiments were stored in PBS at an iron concentration of 1 mg/ml at 4°C and utilized within two weeks. To ensure that SPIONs were endotoxin-free, particles preparations were regularly tested using the Limulus Amebocyte Lysate (LAL) assay (Lonza, Walkersville, MD, USA) performed according to the manufacturer's specifications. None of the particle batches tested was found to contain endotoxin (data not shown).

Human monocyte-derived DC cultures, maturation and SPION exposure

Peripheral blood mononuclear cells (PBMC) were obtained from buffy coats provided by healthy blood donors (Regional Red Cross Blood Donation Centre, Bern, Switzerland) by Ficoll-Paque (Amersham, Biosciences) density centrifugation. Monocytes were isolated from PBMC by CD14 positive selection utilizing the MACS microbeads (Miltenyi Biotech) as per manufacturer protocol to a purity of >95%. The CD14 negative fraction was frozen and kept for T cell stimulation assays (see autologous $CD4^+$ T cell stimulation assay). MDDCs were generated by culturing in RPMI 1640 medium (Invitrogen) containing 10% FCS, (Amimed/BioConcept), 1% L-glutamine (2 mM; Invitrogen), 1% penicillin/streptomycin (100 U/ml; Invitrogen), 10 ng/ml GM-CSF (R&D Systems), and 10 ng/ml IL-4 (R&D Systems) for six days at 37°C in a 5% CO_2 humidified atmosphere as previously described (Sallusto and Lanzavecchia 1994). All reagents utilized were endotoxin-free as per manufacturer standard. To induce maturation, MDDCs were stimulated during 12 h with 100 ng/ml LPS (Sigma-Aldrich) as previously described and exposed during 12 h to SPIONs that were pre-diluted in PBS, cautiously sonicated during 2 min, and directly re-suspended in the cell culture medium at indicated final concentrations (Regamey et al. 2007).

Flow cytometry (FACS)

Unless indicated otherwise, antibodies were obtained from eBioscience. Staining was strictly performed on ice throughout the entire procedure. Cells were incubated with anti-Fc block (anti-human CD16/CD32; BD Pharmingen) to reduce non-specific binding 10 min prior to addition of the following anti-human Abs: PE-conjugated anti-CD11c and -CD123, PE-Cy7-conjugated HLA-DR, biotinylated anti-CD11b -CD80, -CD83, -CD86, -BDCA1 (BD Pharmingen), -BDCA2 (BD Pharmingen). Relevant isotype control antibodies were used throughout. Streptavidin-conjugated fluorochromes, allophycocyanin, PerCP, FITC, PE, and PerCP cyanin 5.5 were purchased from eBioscience. Cell samples were analyzed for surface fluorescence by flow cytometry using a LSRII (BD Biosciences). Unless indicated otherwise, staining for surface molecules was reported as the frequency of cells expressing the marker of interest. Endocytotic capacity (antigen uptake) and antigen processing were measured by incubation with a variety of fluorescent conjugates, as previously described (Wikstrom et al. 2006; von Garnier et al. 2007). OVA-Alexa Fluor 647 (Molecular Probes) was utilized to measure endocytotic capacity and DQ-OVA (Molecular Probes) to determine antigen processing. MDDCs were incubated during a time course of 0–120 min at 37°C or on ice (controls) to measure antigen uptake and processing. Propidium iodide (Invitrogen) and annexin V (eBioscience) staining was performed to determine cell death and apoptosis, respectively. Cells frozen for 30 min at −70°C or fixed with formaldehyde 4% for 30 min at room temperature, served as positive controls for propidium iodide and annexin V staining, respectively (data not shown). FACS data was analyzed using FlowJo (Tree Star).

Autologous $CD4^+$ T cell stimulation assay

Autologous $CD4^+$ T cells were negatively selected from the CD14 negative fraction (see above,

monocyte isolation) utilizing MACS microbeads (Miltenyi Biotech) as per manufacturer protocol to a purity of 98%. After washing, $10 - 10^3$ MDDCs (1.0×10^2 to 1.0×10^4 cells/ml) stimulated with LPS and/or exposed to both PVA-SPION concentrations were incubated with 10^4 $CD4^+$ T cells (1.0×10^5 cells/ml) at DCs to $CD4^+$ T cell ratios of 1:1000 – 1:10 in 96 well tissue culture plates containing 200 µl of medium per well. Tetanus toxoid (Calbiochem) was used as antigen at a concentration of 0.5 µg/ml. Unless indicated otherwise, the results with the 1:10 DC:$CD4^+$ T cell ratio are shown. Co-cultures were performed for five days and pulsed with 0.5 µCi [^{3}H] thymidine (Amersham Biosciences) during the last 16 h. The incorporated radioactivity was measured using a liquid scintillation counter. A separate culture plate without radioactivity was utilized for cytokine determination in the supernatants.

Cytokine assays

Cell culture supernatants from autologous $CD4^+$ T cell stimulation assays were analyzed utilizing a Luminex multiplex array system (Bio-Rad) for IL-1β, IL-6, IL-10, IL-12p70, IFNγ, and TNFα, according to manufacturer protocol.

Quantification of endocytosed SPIONs and co-localization by laser scanning microscopy (LSM) and image restoration

MDDCs were treated with PVA-SPIONs (10 and 20 µg/ml) during 4 h and subsequently incubated with Transferrin Alexa 633 (100 µg/ml; marker for lysosomes) for 20 min either in the absence or presence of cytochalasin D (Cyt-D; 10 µg/ml) added to the cell cultures 30 min before particle exposure as previously described (Thiele et al. 2001). Cells were fixed in 2.5% glutaraldehyde and processed for TEM (see below). For the analysis by LSM, cells were washed in phosphate-buffered saline (PBS, 10 mM, pH 7.4: 130 mMNaCl, Na_2HPO_4, KH_2PO_4) and fixed for 15 min at room temperature in 3% paraformaldehyde in PBS. Fixed cells were treated with 0.1 M glycine in PBS for 5 min and permeabilized in 0.2% Triton X-100 in PBS for 15 min. Cells were stained with rhodamine phalloidin 1:100 (R-415; Molecular Probes, Invitrogen AG, Basel, Switzerland) and with DAPI (1 µg/ml) for 1 h at room temperature.

Optical sections were taken using a Zeiss LSM 510 Meta with an inverted Zeiss microscope (Axiovert 200M; lasers: HeNe 633 nm, HeNe 543 nm, Ar 488 nm, and a 405 nm diode laser; Carl Zeiss AG, Feldbach, Switzerland) with a Plan-Apochromat 63 ×1.4 objective and an optical zoom of 3.5×. The resulting voxel size was 0.08 × 0.08 × 0.25 µm. Image processing, particle visualization and co-localization with lysosomes was performed with IMARIS (Bitplane AG, Zurich, Switzerland), a three-dimensional multi-channel image processing software for confocal microscopic images. To visualize the labelled MDDCs, a rendering mode was used that displays the maximum intensity projection (i.e. the maximum intensity of all layers along the viewing direction) of the recorded three-dimensional stack. After image acquisition, the total particle number and the number of particles co-localized with lysosomes were counted with the particle tracker software Diacount (Semasopht, Lausanne, Switzerland). In each experimental sample the cells were randomly scanned by LSM. Experiments were performed in triplicate or quadruplicate and 10 or more cells were scanned per data point. Since LSM is not able to resolve SPIONs size, counted particles and co-localization were expressed as particle events and co-localized events, respectively with events referring to the number of voxels emitting signals that stem from particles or co-localization (Lehmann et al. 2010).

Transmission electron microscopy (TEM)

MDDCs were fixed with buffered 2.5% glutaraldehyde (Agar Scientific Ltd, Plano GmbH, Wetzlar, Germany), 1.0% osmium tetroxide (Simec, Zofingen, Switzerland), and 0.5% uranyl acetate (Fluka Chemie GmbH, Sigma-Aldrich, Buchs, Switzerland). Subsequently, cells were dehydrated in a graded series of ethanol (70, 80, 96, and 2 × 100%) and gradual replacement of ethanol by propylene oxide before infiltrating and embedding the cells in epoxy resin was performed. Ultrathin sections were obtained utilizing an ultramicrotome (Reichert, Austria), before transfer onto 200-mesh uncoated copper grids stained with uranyl acetate and counterstained with lead citrate. TEM was performed with a Philips 300 TEM at 60 kV (FEI Company Philips Electron Optics, Zurich, Switzerland). Cells from at least three different donors were analyzed. For qualitative analysis sections of 5–10 cells were analyzed per donor.

Statistical analyses

Unless indicated otherwise, data are presented as mean ± SEM of experiments from 3–8 different experiments/donors. Unpaired Student's *t*-tests were applied to calculate significances. Differences

were considered as statistically significant at a value for $p < 0.05$. Data were analyzed using GraphPad Prism software.

Results

PVA-SPION uptake by MDDCs and modulation by concomitant LPS exposure

To quantify PVA-SPION uptake, MDDCs were treated during 12 h with 5–100 μg/ml PVA-SPIONs with or without concomitant LPS (Figure 1). FACS analyses showed that SPION uptake by MDDCs occurred dose-dependently, as measured by an increase in delta mean fluorescence intensity (Figure 1A). Concurrent LPS exposure decreased SPION uptake by MDDCs at concentrations greater than 20 μg/ml by a known phenomenon related to LPS-dependent MDDC maturation that decreases the ability to endocytose antigen (Figure 1B). Based on these dose-ranging studies and importantly to avoid maturation (and LPS)-dependent decrease of nanoparticle uptake by MDDCs, we performed subsequent experiments with PVA-SPIONs only with the two concentrations of 10 and 20 μg/ml.

Morphological analyses and quantification of SPION uptake by MDDCs

To further characterize the fate of PVA-SPIONs taken up by MDDCs, morphological analyses were performed by TEM and LSM (Figure 2). TEM enabled identification of electron-dense iron cores (10 nm in diameter), but not PVA shells, of individual PVA-SPIONs (Figure 2A). In TEM analyses of MDDCs, intra-cellular PVA-SPIONs were surrounded by a membranous structure corresponding to the endosomal compartment (Figure 2B and insert). Treatment of MDDCs with cytochalasin D to inhibit actin-dependent endocytosis resulted in extra-cellular accumulation of PVA-SPIONs and a sharp decline of intra-cellular PVA-SPIONs (Figure 2C and insert). LSM was performed on MDDCs to further characterize uptake, intracellular localization, and association of PVA-SPIONs with the endosomal compartment (Figure 2D–I). Cytochalasin D treatment of MDDCs resulted in fewer cytoplasmic processes through inhibition of actin polymerization and strongly reduced particle uptake, as shown both in TEM and LSM images (Figure 2B, D, E, G, I).

Since conventional LSM is not able to resolve individual PVA-SPIONs (showing diameters of 100 nm and smaller) which are located below the theoretical limit of resolution of light microscopy (around 200 nm), counted particles and co-localization were expressed as particle events and co-localized events, respectively with events referring to the number of voxel emitting signals that stem from particles or co-localization (expressed as number of particle events in Figure 3; see also *Materials and methods* section). Several salient findings emerged

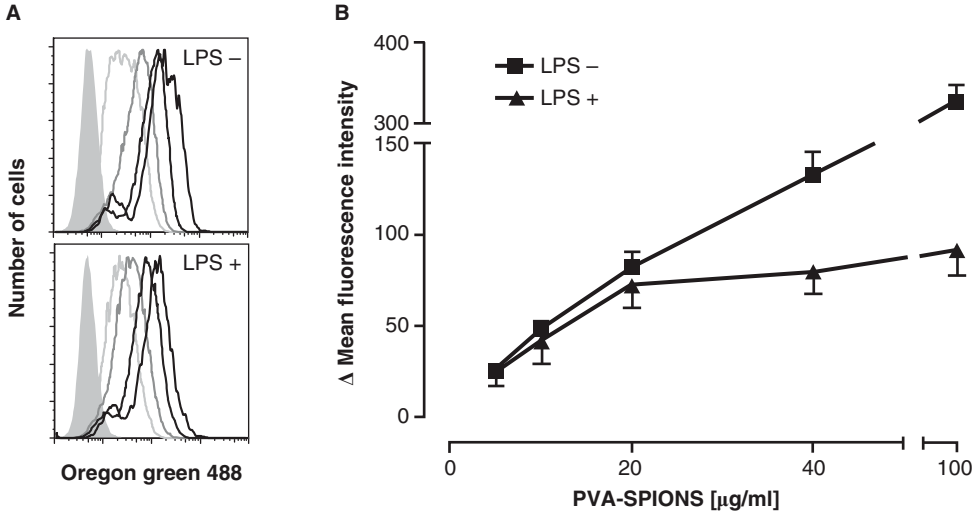

Figure 1. Flow-cytometric (FACS) analysis of PVA-SPION uptake by MDDCs. MDDCs were incubated during 12 h with different concentrations of Oregon green 488-labelled PVA-SPIONs in the presence or absence of LPS. (A) FACS histogram plots gated on the MDDC population (see Figure 4a or Figure 5a) in the absence (upper panel, LPS −) or presence (lower panel, LPS +) of LPS with 0 μg/ml (grey solid curve), 10 μg/ml (faint grey line), 20 μg/ml (light grey line), 40 μg/ml (dark grey line), and 100 μg/ml (black line) of SPIONs. One representative graph of three independent experiments (different donors) is shown. (B) SPION uptake by MDDCs as delta mean fluorescence intensity (measured MFI in MDDCs treated with PVA-SPIONs minus background MFI in untreated MDDCs) at different SPION concentrations tested. Average values (± SEM) of three experiments that originate from three different donors are shown.

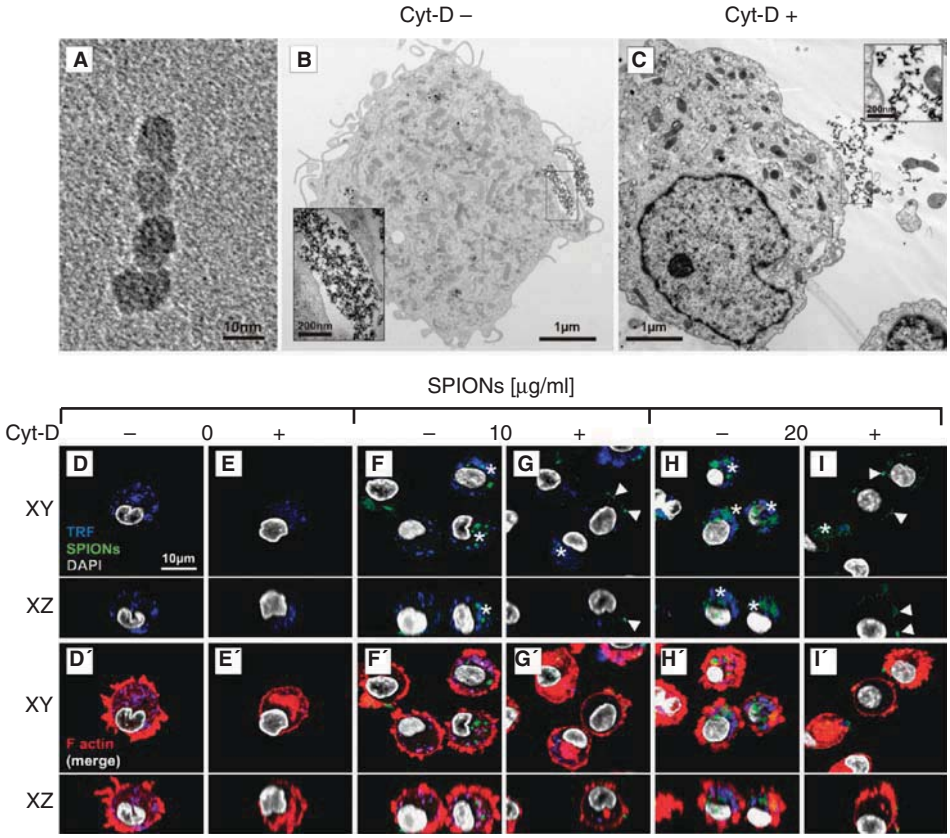

Figure 2. Visualization of PVA-SPION uptake by MDDCs with TEM and LSM as described in the *Methods* section. MDDCs were treated with PVA-SPIONs (10 and 20 µg/ml) during 4 hours and subsequently incubated with Transferrin Alexa 633 (100 µg/ml; marker for lysosomes) for 20 min either in the absence or presence of cytochalasin D (Cyt-D; 10 µg/ml) added to the cell cultures 30 min before particle exposure as previously described (Thiele et al. 2001). (A–C) TEM pictures of individual PVA-SPIONs (A), MDDCs without (B) and with (C) cytochalasin D pre-treatment prior to incubation with PVA-SPIONs. Higher magnification inserts show PVA-SPIONs intra-cellularly in lysosomes (B), or extra-cellularly (C). (D-I) LSM pictures of MDDCs treated with Oregon green labelled PVA-SPIONs (D and E, 0 µg/ml; F and G, 10 µg/ml; H and I; 20 µg/ml) during 4 h with transferrin Alexa 633 for the last 20 min either in the absence (D, F, and H) or presence (E, G, and I) of cytochalasin D. Micrographs (D-I) show the localization of PVA-SPIONs (green), transferrin receptor (blue), and nuclei (white) in different experimental conditions. Actin (red) staining (D'-I') facilitated detection of intra-cellular (asterisks) and extra-cellular (arrowheads) localization of SPIONs. xy-projections (top panels) and xz-projections (lower panels) were obtained from multiple consecutive optical sections. One representative experiment from three experiments is shown.

from quantitative LSM analyses (Figure 3). First, there was a significant dose-dependent increase of intra-cellular particle events in MDDCs (no cytochalasin D) when increasing the PVA-SPION concentration from 10–20 µg/ml (Figure 3; intra-cell. in Cyt D –). Second, co-localization of particle events and endosomal compartment (transferrin receptor staining) remained constant at both concentrations tested (Figure 3; co-local. in Cyt D –), but proportionally more events were co-localized (total intracellular particle events/co-localized events) with 10 µg/ml (61%) than for 20 µg/ml (43%) (data not shown). Third, treating MDDCs with cytochalasin D led to significantly reduced intra-cellular and co-localized particle events, but increased extra-cellular particle events, i.e. corresponding to particle aggregates attached to the outer cell surface (Figure 3; extra-cell. Cyt D +). A degree of extra-cellular particle aggregation may have led to a reduced total number of particle (fluorescence) events counted, as compared to fluorescence emitted by non-aggregated particles. It is necessary to emphasize that extra-cellular particle events counted in cytochalasin D-treated cells comprise only particles attached to the cellular surface and therefore do not represent the complete amount of particles restricted from entering the cells (hence the smaller amount of overall particle events counted in cytochalasin D-treated cells).

In summary, TEM and LSM studies showed that PVA-SPIONs were endocytosed in a dose-related manner, predominantly by an actin-dependent process. Very few particles entered MDDCs by other, non-actin-dependent processes, as shown by the number of particle-related events that occurred after

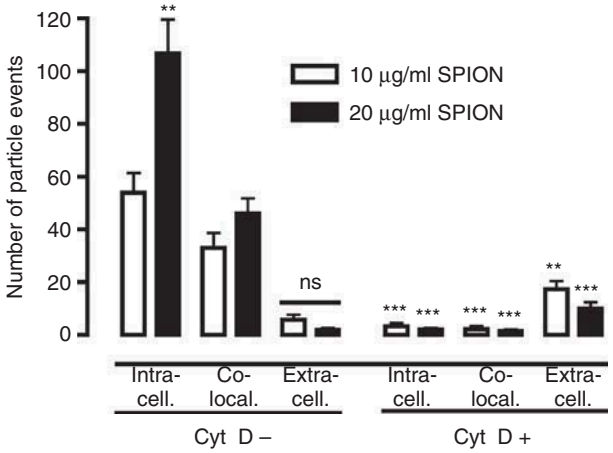

Figure 3. Fate of PVA-SPIONs incubated with cytochalasin D-treated (Cyt D +) or –untreated (Cyt D –) MDDCs as determined by LSM. MDDCs were treated with PVA-SPIONs (10 and 20 µg/ml) during 4 h and subsequently incubated with Transferrin Alexa 633 (100 µg/ml; marker for lysosomes) for 20 min either in the absence or presence of cytochalasin D (Cyt-D; 10 µg/ml) added to the cell cultures 30 min before particle exposure as previously described (Thiele et al. 2001) PVA-SPIONs were localized either extra-cellular (extra-cell.), or intra-cellular (intra-cell.), and co-localized (co-local.) with transferrin receptor staining for the latter. Quantification was performed as described in the *Methods* section. Bar graph represents the mean (± SEM) from four experiments. For statistics, $*p < 0.05$; $**p < 0.005$; $***p < 0.0005$; and ns, non-significant as determined by unpaired Student's *t*-test comparing cytochalasin D-untreated (Cyt D –) vs. cytochalasin-treated (Cyt D +) MDDCs, except for "intra-cell" and "co-local" in untreated MDDCs (Cyt D –), where 10 µg/ml vs. 20 µg/ml SPIONs were compared.

cytochalasin D pharmacological blockade. Depending on their initial concentration, between 40 and 60% of the intra-cellular PVA-SPIONs trafficked to the endosomal compartment, as shown by co-localization studies.

Phenotypic changes, apoptosis, and cell death in MDDCs treated with PVA-SPIONs

FACS analyses were performed to assess the surface phenotypic changes on MDDCs following exposure to 10 and 20 µg/ml SPIONs with or without concurrent LPS (Figure 4). These PVA-SPION doses were chosen because LPS treatment did not alter the PVA-SPION uptake at such concentrations (see above and Figure 1). The gating strategy utilized is shown with a representative experiment (Figure 4A). The frequency of MHC class II and co-stimulatory molecule CD80/CD86 expression increased with LPS treatment but was not affected by PVA-SPION treatment except for cell cultures exposed to 10 µg/ml PVA-SPIONs that showed lower MHC II expression with and without LPS activation (Figure 4B). Furthermore, as a marker of maturation, CD83 remained unchanged when MDDCs were treated with PVA-SPIONs, both with (consistent maturation of DCs) and without LPS (Figure 4B). The frequencies for $CD11c^+$ $BDCA\text{-}1^+$ myeloid DC (mDC) or the fraction of $CD123^+$ $BDCA\text{-}2^+$ plasmacytoid (pDC) were not altered by PVA-SPION treatment (Figure 4B). Importantly, no excess apoptosis (Annexin V) or necrosis (propidium iodide) was observed in MDDCs treated with PVA-SPIONs (Figure 4B). Treatment with PVA-SPION concentrations up to 50 µg/ml did not affect MDDC phenotype or viability (data not shown).

In summary, these data provide evidence that in treated MDDCs, PVA-SPIONs did not induce maturational or activation changes (except a lower frequency of MHC II^+ MDDCs treated with 10 µg/ml PVA-SPIONs), alter the mDC/pDC balance, or cause apoptosis/cell death. Furthermore, responses of MDDC to LPS activation remained intact during treatment with PVA-SPIONs.

Exposure to PVA-SPIONs: functional changes in MDDCs

A further series of experiments investigated whether MDDCs underwent functional changes by PVA-SPION treatment. To assess the capacity of MDDCs for antigen uptake and antigen processing, two fluorochrome compounds coupled to ovalbumin (OVA) as a carrier protein were utilized: OVA-Alexa 647 and DQ-OVA as surrogate markers for antigen uptake and antigen processing, respectively (Wikstrom et al. 2006; von Garnier et al. 2007). The FACS gating strategy utilized to determine these parameters is detailed in Figure 5A. Surface expression of MHCII, a prerequisite for antigen-presentation, was also determined simultaneously during incubation with the above fluorochrome compounds.

Treatment with PVA-SPIONs did not alter the capacity of MDDCs to endocytose antigen, but down-regulated the ability for antigen processing at higher PVA-SPION concentration (20 µg/ml), both with and without concomitant LPS exposure (Figure 5B, left and centre panels). Moreover, during the time course (0–120 min) performed for antigen uptake and antigen processing experiments, SPIONs-treated MDDCs showed less LPS-induced MHCII surface expression (Figure 5B, right panels).

To determine how changes in antigen processing and MHCII expression impacted on downstream immune responses, an *in vitro* $CD4^+$ T cell stimulation assay was utilized as described in the *Methods* section (Figure 6). Following treatment with PVA-SPIONs, MDDCs were co-cultured with autologous $CD4^+$ T cells to assess the responses to LPS, antigen

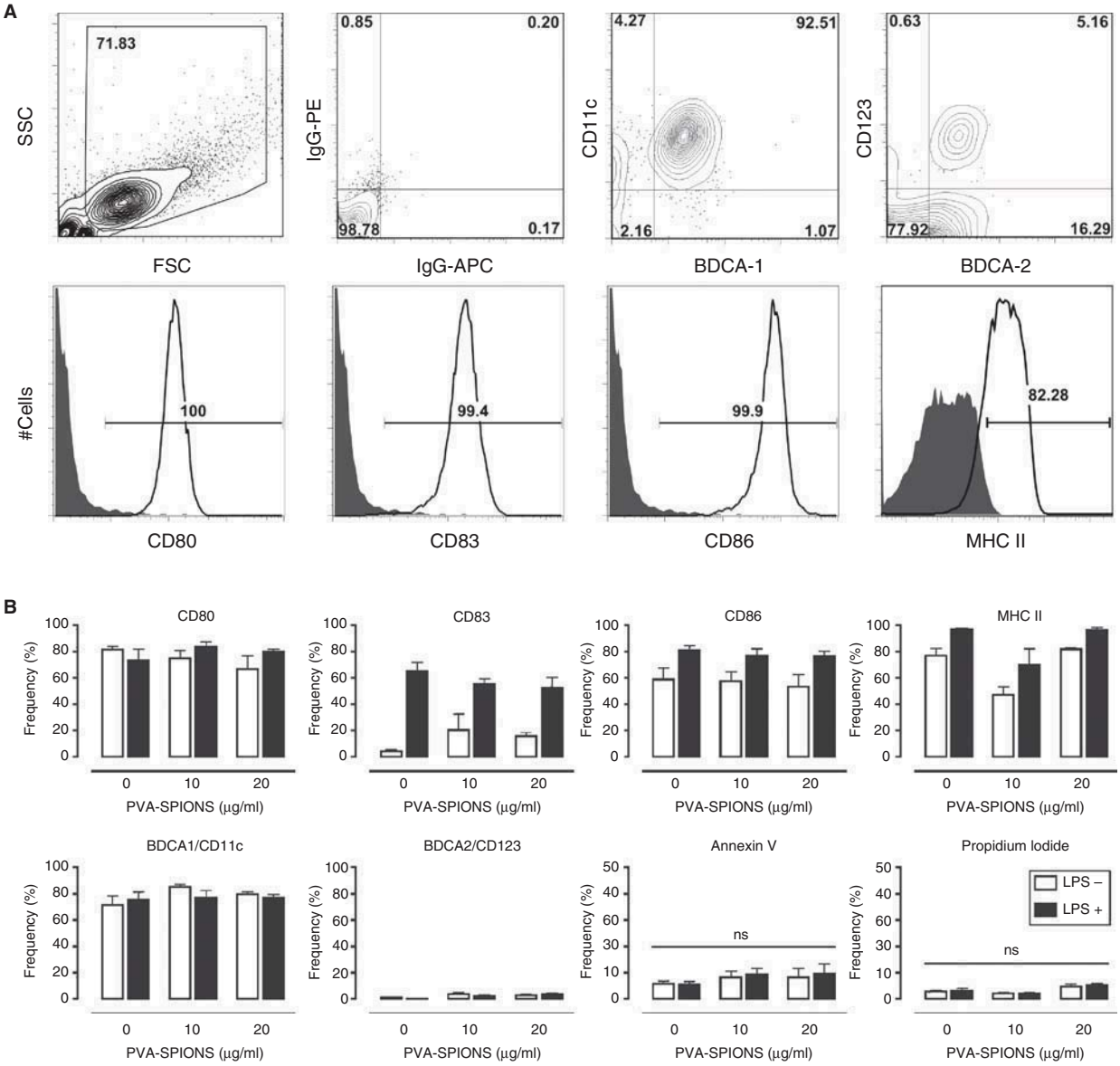

Figure 4. Surface phenotype, apoptosis, and cell death of MDDCs following treatment with PVA-SPIONs during 12 h. (A) Representative experiment showing gating strategy based on relevant isotype controls (IgG, and filled histogram curves) to determine frequency of expression for surface markers: activation (CD80, CD86), maturation (CD83), myeloid or conventional DCs (BDCA1/CD11c), plasmacytoid DCs (BDCA2/CD123). (B) MDDCs were treated with 0, 10, and 20 μg/ml PVA-SPIONs in the absence (open bars, LPS −) or presence (filled bars, LPS +) of LPS as detailed in the methods section. Bar graphs (average ± SEM) show the frequency of surface marker expression, apoptosis (Annexin V), and cell death (Propidium iodide). Results from five experiments are shown and expressed as mean (± SEM). ns, non-significant and $*p < 0.05$ as determined by unpaired Student's *t*-test comparing PVA-SPION-untreated vs. PVA-SPION-treated MDDCs.

(tetanus toxoid), or both (Figure 6). Both PVA-SPION concentrations significantly reduced $CD4^+$ T cell proliferation induced by LPS, tetanus toxoid, or both combined (Figure 6). As T cell stimulations were reduced for both PVA-SPION concentrations, we determined cytokine levels for 10 and 20 μg/ml - PVA-SPIONs (Figure 7). Cytokines measured in supernatants obtained from co-culture experiments (i.e. 10 and 20 μg/ml PVA-SPION-treated MDDCs and $CD4^+$ T cells) in the presence LPS and tetanus toxoid showed a significantly decreased release of IL-1β, IL-5, IL-6, IL-12p70, TNF-α, and IFN-γ, but increased production of IL-10 (Figure 7).

Discussion

Development of biomedical nanoparticles for future diagnostic and therapeutic applications is currently an area of intense research in nanotechnology. Nanosized formulations can be specifically designed

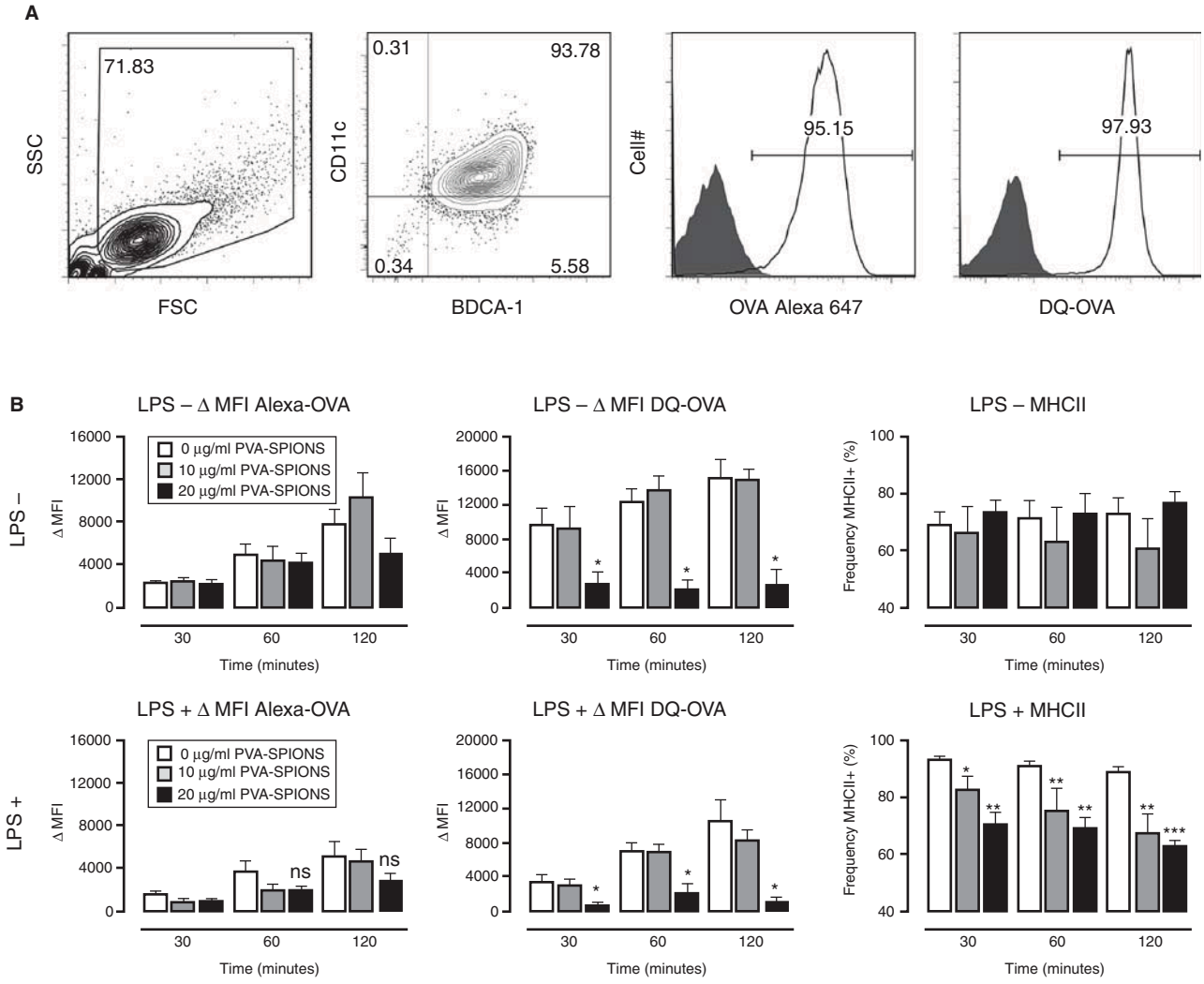

Figure 5. Antigen-uptake, antigen-processing, and MHCII expression of MDDCs treated with PVA-SPIONs during 12 h. Endocytotic capacity (antigen uptake) and antigen processing were measured by incubation with a variety of fluorescent conjugates, as previously described (Wikstrom et al. 2006; von Garnier et al. 2007). OVA-Alexa Fluor 647 (Alexa-OVA) was utilized to measure endocytotic capacity and DQ-OVA to determine antigen processing. MDDCs were incubated during a time course of 0–120 min at 37°C or on ice (controls) to measure antigen uptake and processing. (A) Gating strategy consists in an initial FSC/SSC gate (panel one from left), isotype-controlled gate for $CD11c^+/BDCA1^+$ DCs (panel two from left), and Alexa-OVA^+ (antigen uptake) or DQ-OVA^+ (antigen processing) cells (panel three and four from the left). Negative controls (solid curves) in the histogram plots were derived from cells kept at 4°C during the length of the experiment. (B) Bar graphs (white, 0 μg/ml; grey, 10 μg/ml; and black 20 μg/ml PVA-SPIONs) show the capacity for antigen-uptake (left panels, Alexa-OVA), antigen processing (middle panels, DQ-OVA), and expression of MHCII (right panels, MHCII). Results from five experiments are shown and expressed as average Delta mean fluorescence intensity (Δ MFI = measured MFI − background of isotype control MFI) values ± SEM. $^*p < 0.05$; $^{**}p < 0.005$; and $^{***}p < 0.0005$ as determined by unpaired Student's *t*-test comparing PVA-SPION-treated MDDCs to untreated MDDCs.

to either stimulate or inhibit immune responses, or evade recognition by the immune system altogether. Nanomaterials administered to the organism will potentially encounter antigen-presenting cells, especially DCs, that may undergo functional changes with profound consequences on the initiation and subsequent regulation of immune responses to nanoparticles or their payload. Alteration of immune responses by nanoparticles may represent a form of "nano-immuno-toxic" effect that may seriously undermine future efforts to develop novel therapeutic or diagnostic approaches.

Utilizing prototypic fluorochrome-labelled model PVA-SPIONs previously evaluated in several preclinical studies, we herein provide data derived from *in vitro* studies of DCs treated with such nanoparticles (Petri-Fink et al. 2005; Cengelli et al. 2006; Hellstern et al. 2006; Petri-Fink and Hofmann 2007; von Zur Muhlen et al. 2007; Butoescu et al. 2008; Petri-Fink et al. 2008; Butoescu et al. 2009;

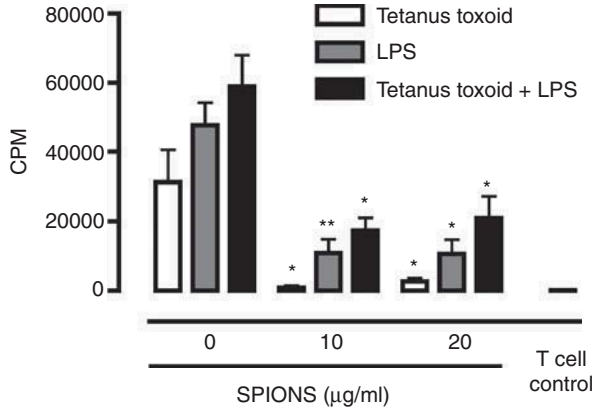

Figure 6. $CD4^+$ T cell stimulatory capacity of MDDCs treated with PVA-SPIONs. MDDCs were treated with 10 μg/ml and 20 μg/ml of PVA-SPIONs during 12 h in the absence or presence of LPS. As detailed in the methods section, MDDCs were subsequently incubated with autologous $CD4^+$ T cells to determine antigen-specific (tetanus toxoid) and/or LPS-dependent (LPS) $CD4^+$ T cell proliferation. Co-cultures were performed for five days and pulsed with 0.5 μCi [^{3}H] thymidine during the last 16 h. For T cell control, culture was performed without MDDCs to determine background T cell proliferation. Results from five experiments are shown and expressed as average values ± SEM. For statistics, $^\star p < 0.05$ and $^{\star\star} p < 0.005$ as determined by unpaired Student's *t*-test comparing PVA-SPION-exposed to non-exposed MDDCs. CPM: counts per minute.

Montet-Abou et al. 2010). Other research groups have previously investigated effects of nanoparticles on DC activation and maturation, but to our knowledge, our data are the first to show that prototypic biomedical nanoparticles, such as SPIONs, are able to modulate immune responses by affecting DC-dependent antigen-processing and antigen-presentation. Broos et al. (2010) recently showed that 200 nm-sized biodegradable poly(γ-glutamic acid) (γ-PGA) nanoparticles activated immature MDDCs through increased expression of co-stimulatory molecules and secretion of inflammatory chemokines and cytokines; in MDDCs obtained from grass pollen allergic individuals, γ-PGA nanoparticles increased allergen-specific IL-10 production. A fullerene derivative containing an entrapped Gadolinium atom (Gd@C82(OH)22) activated DCs and in mice enhanced ovalbumin-specific Th1 responses (Yang et al. 2010). Furthermore, Vallhov et al. (2007) compared the effects of different sized mesoporous silica particles (270 nm 2.5 μm) on the viability and the activation markers of human DCs and found that the smaller particles affected the cells to a minor degree compared to the larger particles. The most salient findings from our work showed that *in vitro* treatment of MDDCs with PVA-coated SPIONs did not affect maturation, activation, or viability of DCs, but modulated their capacity to process and present antigen, leading to decreased T cell stimulation and less pro-inflammatory cytokine release.

In the first part of our studies we provided advanced imaging data obtained from TEM and LSM showing that MDDCs endocytosed PVA-SPIONs mainly by an actin-dependent mechanism, with subsequent trafficking of PVA-SPIONs to the endosomal compartment. Although the number of intra-cellular particles was dependent on the PVA-SPION concentration, localization to the endosomal compartment was constant and unaffected by PVA-SPION concentration. Furthermore, particle uptake was almost completely blocked when cells were treated with cytochalasin D, an inhibitor of actin polymerization. Since there is no data yet available on SPION uptake by DCs, our *in vitro* data should be compared to similar studies performed with different cell types. As an example, Landmark et al. (2008) exposed a carcinoma cell line to organic-coated super-paramagnetic iron oxide nanoparticles and observed frequent uptake within intracellular vesicles. Furthermore, due to a high autocorrelation between intra-cellular zinc and iron, the authors postulated an uptake mechanism through clathrin-coated pits, because zinc is a transmission metal typically associated with this mechanism of endocytosis. Since uptake via clathrin-coated pits is an actin-driven process, these findings are in accordance with our results in DCs. Although LSM data provided only a 40–60% co-localization rate between PVA-SPIONs and the transferrin receptor fluorescence, our TEM studies failed to detect SPIONs localized freely in the cytoplasm (outside endosomes), nor in the nucleus or in mitochondria. This finding is of particular importance since we can assume that the PVA-SPIONs utilized in our study are unlikely to interact with genomic DNA in the nucleus or with respiratory chain components in mitochondria and are therefore less likely to induce genetic changes, inflammatory effects, and/or oxidative stress. Furthermore, in particle-exposed cell cultures we failed to detect an increase in cell death or apoptosis that would be an inevitable outcome of enhanced cytotoxicity. In an *in vitro* study utilizing a triple cell co-culture model of the lung mucosa (consisting of epithelial A549 cells, human monocyte-derived macrophages, and DCs), 25 nm gold nanoparticles were freely distributed within the cytoplasm and cell nuclei (Rothen-Rutishauser et al. 2007). Contrasting with other types of nanoparticles (polystyrene, TiO_2) that were detected intra-cellular only within membrane bound vesicles, gold nanoparticles induced an enhanced release of TNFα in triple cell co-cultures. In-depth analysis assessing intracellular distribution of PVA-SPIONs will eventually be necessary, e.g. by utilizing advanced imaging methods such as electron

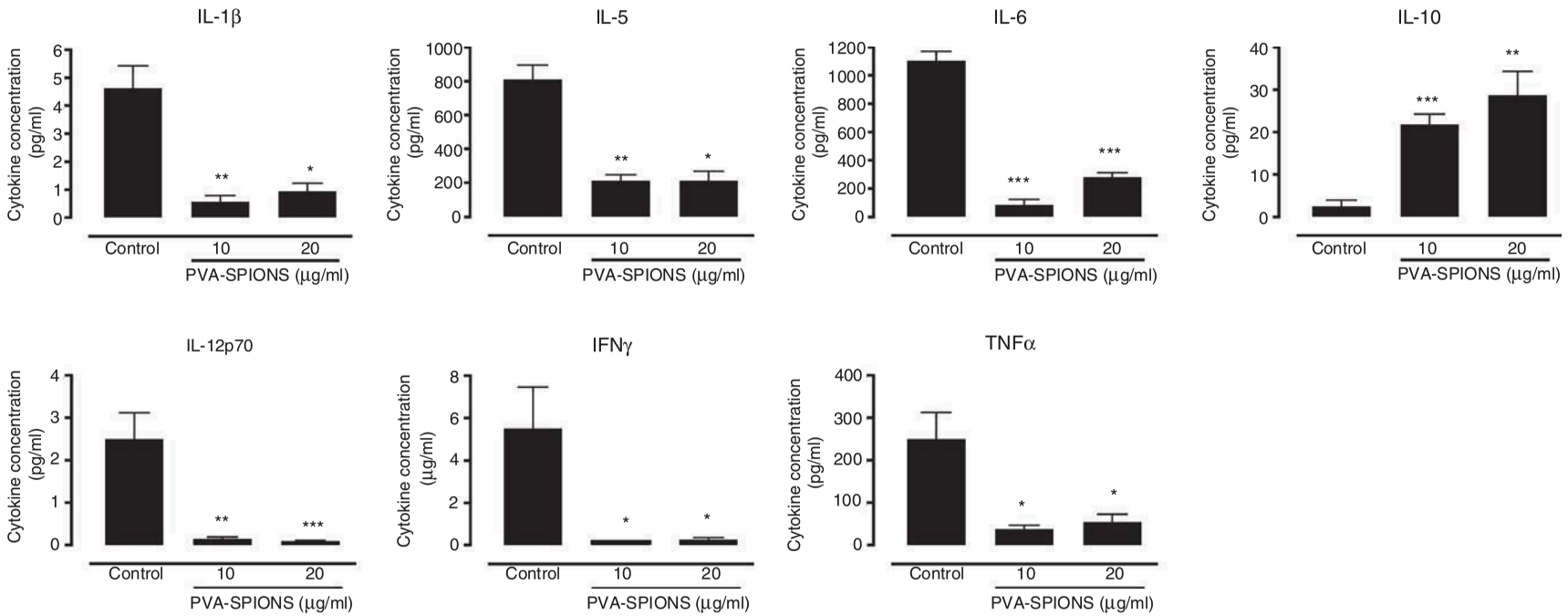

Figure 7. Cytokine concentrations in supernatants obtained from $CD4^+$ T cell stimulatory assays. MDDCs were treated with 10 and 20 µg/ml PVA-SPIONs for 12 h in the presence of LPS. As detailed in the *methods* section, MDDCs were subsequently incubated with autologous $CD4^+$ T cells to determine antigen-specific (tetanus toxoid) and LPS-dependent cytokine production. Co-cultures were performed for five days. Results from 3–4 experiments are shown and expressed as mean cytokine concentrations ± SEM. Control cultures (with LPS + TT) were not treated with PVA-SPIONs. All cytokine changes were significant as determined by unpaired Student's *t*-test comparing MDDCs treated with PVA-SPIONs to untreated MDDCs; $^{\star}p < 0.05$; $^{\star\star}p < 0.005$; and $^{\star\star\star}p < 0.0005$.

energy loss spectroscopy or tomography EM to conclusively determine if PVA-SPIONs have the potential to enter mitochondria and/or cell nuclei (Rothen-Rutishauser et al. 2007). Another important issue, i.e. investigation of SPION biodegradation in DCs, was beyond the scope of our present work; but several lines of evidence in the literature suggest that a certain degree of SPION degradation is likely to occur via the lysosomal pathway: A study on murine bone marrow macrophages showed that opsonized albumin and dextran-coated SPIONs taken up by receptor-mediated endocytosis were found in vesicles resembling terminal lysosomes (Schulze et al. 1995).

Another study using mesenchymal stem cells exposed to dextran-coated SPIONs found particle-containing endosomes to fuse with lysosomes, leading to degradation of SPIONs into soluble Fe(III) within the lysosomes (Arbab et al. 2005). Several toxicological studies have demonstrated over the last decade that combustion generated nanoparticles readily generate oxidative stress through reactive oxidative species (ROS) and inflammation (Donaldson et al. 2005; Xia et al. 2006; Warheit et al. 2007). In addition to the fact that some nanoparticles are able to directly interact with genomic DNA, it has been shown that oxidative stress may play a major role in particle-induced DNA damage that can be prevented by antioxidants and scavengers of ROS (Donaldson et al. 2003; Tsoli et al. 2005). However, detailed molecular mechanisms involved in the hallmark cellular responses to genotoxic effects are currently not known and require meticulous clarification in the future.

The decreased antigen processing capability of MDDCs with PVA-SPION treatment may be partly explained by the fact that DCs have a limited proteolytic capacity in their lysosomes that is enhanced with maturation (Trombetta et al. 2003; Trombetta and Mellman 2005). A central question when investigating interactions between cells and nanoparticles is the colloidal behaviour of the latter, as this will ultimately determine how cells "sense" particles and respond to these. Though we cannot exclude a certain degree of agglomeration of PVA-SPIONs localized within the lysosomes occurred prior to endocytosis, previous investigations by Petri-Fink and Hofmann (2007) concluded that the cell culture medium (i.e. DMEM or RPMI) had no influence, but addition of serum to the cell culture medium significantly reduced the agglomeration rate of PVA-SPIONs. Based on these data, utilization of RPMI plus FCS as culture medium in our *in vitro* experiments reduced agglomeration rates of PVA-SPIONs. Once endocytosed, PVA-SPIONs may simply undergo a concentration effect within lysosomes. Although electron micrographs showed PVA-SPION agglomerates in the lysosomes, we have not investigated whether particles underwent specific structural changes following endocytosis. Although it will be crucial for the development of nanoparticles destined for specific applications to determine changes that particles may undergo within different intra-cellular compartments (e.g. lysosomes), this is beyond the scope of the current report and will require clarification in future work.

In the second part of our studies, flow cytometric analyses provided evidence that PVA-SPIONs did not affect MDDC maturation, activation, frequencies of mDC and a minor fraction of pDC, or cell viability. In contrast, SPIONs modulated MDDC function by decreasing antigen processing, expression of MHCII and the capacity to stimulate autologous $CD4^+$ T cells *in vitro*. These findings suggest that PVA-SPIONs possess an intrinsic capacity for immune-modulation and may potentially provide a form of tolerance induction by affecting DC function. There are several lines of evidence in the literature demonstrating that other types of nanoparticles may induce a degree of desirable immune-suppression: synthetic peptide dendrimers inhibited experimental allergic encephalomyelitis, allergen-loaded nanoparticles and dendrimers down-regulated allergic reactions to environmental and food allergens, and a fullerene derivative polyhydroxy C60 prevented type I hypersensitivity reactions (Scholl et al. 2004; Balenga et al. 2006; Gomez et al. 2007, 2008; Wegmann et al. 2008). Size, surface charge and coating may confer to a nanoparticle its intrinsic properties that may lead to immune-suppression. By which mechanisms these effects occur and which immune cells are involved in the process of such an immune-modulation is unclear at present. We herein provide evidence that part of this mechanism may operate via functional modulation of DCs, i.e. by modifying the way that antigen is handled. This may be affected at several levels: First, although our data did not show any changes in antigen uptake by SPION exposure, several other studies showed that this parameter was affected by nanoparticle exposure in phagocytic cells such as macrophages (Moss and Wong 2006). Second, antigen processing as measured with the surrogate marker DQ-OVA, was decreased by SPION exposure. We have previously shown that DQ-OVA-related fluorescence correlates with T cell stimulatory capacity in mouse studies (Wikstrom et al. 2006). Third, expression of MHCII, a prerequisite for efficacious antigen processing, was down-regulated by SPIONs. Consequently, DC-dependent stimulation of autologous $CD4^+$ T cells in the presence of antigen (tetanus toxoid), LPS, or both was reduced by treatment with SPIONs. Cytokine levels measured in T cell simulation assays substantiated the above observations with the finding

that PVA-SPION-treated MDDCs induced significantly lower production of pro-inflammatory cytokines. As an exception IL-10, a cytokine known for its anti-inflammatory effects, was elevated following PVA-SPION treatment relative to the other pro-inflammatory cytokines analysed. Thus PVA-SPIONs may modulate DC function through an intrinsic anti-inflammatory effect and it is unlikely that the observed shift in the pro-/and anti-inflammatory cytokine profiles is due to a generally reduced protein synthesis and/or cytokine production. Moreover, the finding that IFNγ production was strongly reduced further supports that an anti-inflammatory effect of PVA-SPIONs may be present. IFNγ is a type-II interferon secreted by several immune cells (DCs, Th1, T cells, and NKT) with anti-viral, anti-tumor, and immunoregulatory effects induced through regulation of about 30 genes (Schroder et al. 2004). IFNγ regulates class II antigen presentation through the expression of key genes related to MHCII-dependent antigen-presentation: α1, α2, β1, β2 MHC II chains (constituents of the heterodimeric MHC II complex), invariant Ii chain (transmembrane chaperone that traffics MHC II from the endoplasmic reticulum to the MHC II endosomal compartment), DMA and DMB (dimers forming DM, a protein that removes CLIP from the peptide-binding cleft of MHC II so that it is accessible for peptide loading), Cathepsins B, H, L (lysosomal proteases that produce peptides for loading on MHC II), and Class II transactivator (transactivator regulating the transcription of key genes involved in MHC II expression, including constituents of the MHC II complex, Ii chain, and DM) (Lafuse et al. 1995; Lah et al. 1995; Wolf and Ploegh 1995; Mach et al. 1996). Therefore, lower levels of IFNγ release observed in the co-culture assays may reflect the reduced ability of PVA-SPION-treated DCs to present antigen via the MHCII pathway and activate $CD4^+$ T cells.

Finally, reduced capacity of MDDCs to process antigen, secrete cytokines, and stimulate T cells may be partly related to the polymer coating PVA known to bind proteins through hydrogen-bonding interactions (Aggarwal et al. 2009). The extent of protein adsorption is related to its structure and net charge, i.e. negatively charged nanoparticles bind proteins with isoelectric points greater than 5.5, whereas positively charged particles bind proteins with isoelectric points less than 5.5 (Aggarwal et al. 2009). The zeta potential (surface charge) of PVA-SPIONs utilized was slightly positive, therefore binding of proteins with isolelectric points > 5.5 involved in antigen-processing pathways, such as Cathepsin B, H, L1 and DMB might have affected antigen-processing, presentation and T cell stimulation. Binding of the antigen tetanus toxin (isoelectric point 5.8) utilized in the experimental set-up may sequester antigen and interfere with its downstream processing and memory immune responses. Furthermore, interference with inflammatory mediators, such as cytokines, may occur and contribute to strongly decreased levels of IFNγ (isoelectric point 9.5) observed in MDDCs treated with PVA-SPIONs. Whether the extent of PVA-SPION-dependent binding of proteins or enzymes is sufficient to affect DC function is unknown at present and beyond the scope of this study, but will ultimately require careful investigation to understand the immune effects of biomedical nanoparticles.

In summary, data herein reported show to our knowledge for the first time that polymer-coated PVA-SPIONs exerted a certain degree of immune-modulation by inhibition of MDDC function. These effects were mediated by modulation of the antigen-processing and antigen-presentation capacity of MDDCs, resulting in reduced $CD4^+$ T cell activation and altered cytokine profiles towards an anti-inflammatory phenotype dominated by IL-10 production. The observed functional changes indicate that DCs may revert to a more unresponsive and immature-like state (low capacity for T cell stimulation) with PVA-SPION treatment. Although such a functional DC phenotype may be beneficial for the induction of tolerance in various clinical conditions such as autoimmune or allergic disease, consequences of altered immune responses related to nanoparticle treatment will require meticulous clarification. Hence, future strategies to design biomedical nanoparticles for specific therapeutic and diagnostic clinical applications need to take into account their potential effects on key immune cells and downstream immune responses.

Acknowledgements

We gratefully acknowledge the helpful discussions provided by Dr Amiq Gazdhar, critical reading of the manuscript by Dr Phil Stumbles, as well as expert technical assistance provided by Ursula Gerber and Patrizia Castiglioni.

Declaration of interest: Grant-in-aid from the Department of Clinical Research, Bern University Hospital and research grant from the Swiss Society for Pulmonology (CvG), as well as Swiss National Science Foundation Grants No. 320030–122355 (CvG) and No. 205321–120161 (APF). The authors report no conflict of interest. The authors alone are responsible for the content and writing of the paper.

References

Aggarwal P, Hall JB, McLeland CB, Dobrovolskaia MA & McNeil SE. 2009. Nanoparticle interaction with plasma proteins as it relates to particle biodistribution, biocompatibility and therapeutic efficacy. Adv Drug Deliv Rev 61:428–437.

Balenga NA, Zahedifard F, Weiss R, Sarbolouki MN, Thalhamer J & Rafati S. 2006. Protective efficiency of dendrosomes as novel nano-sized adjuvants for DNA vaccination against birch pollen allergy. J Biotechnol 124:602–614.

Baumgartner CE. 1987. Spectrophotometric determination of polyvinyl-alcohol in cadmium hydroxide pastes. Analytical Chemistry 59:2716–2718.

Bee A, Massart R & Neveu S. 1995. Synthesis of very fine maghemite particles. J Magn Magn Mater 149:6–9.

Boyer C, Whittaker M R, Bulmus V, Liu J & Davis TP. 2010. The design and utility of polymer-stabilized iron-oxide nanoparticles for nanomedicine application. NPG Asia Mater 2:23–30.

Broos S, Lundberg K, Akagi T, Kadowaki K, Akashi M, Greiff L, et al. 2010. Immunomodulatory nanoparticles as adjuvants and allergen-delivery system to human dendritic cells: implications for specific immunotherapy. Vaccine 28:5075–5085.

Butoescu N, Jordan O, Burdet P, Stadelmann P, Petri-Fink A, Hofmann H, et al. 2009. Dexamethasone-containing biodegradable superparamagnetic microparticles for intra-articular administration: physicochemical and magnetic properties, in vitro and in vivo drug release. Eur J Pharm Biopharm 72:529–538.

Butoescu N, Jordan O, Petri-Fink A, Hofmann H & Doelker E. 2008. Co-encapsulation of dexamethasone 21-acetate and SPIONs into biodegradable polymeric microparticles designed for intra-articular delivery. J Microencapsul 25:339–350.

Cengelli F, Maysinger D, Tschudi-Monnet F, Montet X, Corot C, Petri-Fink A, et al. 2006. Interaction of functionalized superparamagnetic iron oxide nanoparticles with brain structures. J Pharmacol Exp Ther 318:108–116.

Chastellain M, Petri A & Hofmann H. 2004. Particle size investigations of a multistep synthesis of PVA coated superparamagnetic nanoparticles. J Colloid Interface Sci 278:353–360.

Chen BX, Wilson SR, Das M, Coughlin DJ & Erlanger BF. 1998. Antigenicity of fullerenes: antibodies specific for fullerenes and their characteristics. Proc Natl Acad Sci USA 95:10809–10813.

Dobrovolskaia MA, Aggarwal P, Hall JB & McNeil SE. 2008. Preclinical studies to understand nanoparticle interaction with the immune system and its potential effects on nanoparticle biodistribution. Mol Pharm 5:487–495.

Dobrovolskaia MA, Germolec DR & Weaver JL. 2009. Evaluation of nanoparticle immunotoxicity. Nat Nanotechnol 4:411–414.

Dobrovolskaia MA & McNeil SE. 2007. Immunological properties of engineered nanomaterials. Nat Nanotechnol 2:469–478.

Donaldson K, Stone V, Borm PJ, Jimenez LA, Gilmour PS, Schins RP, et al. 2003. Oxidative stress and calcium signaling in the adverse effects of environmental particles (PM10). Free Radic Biol Med 34:1369–1382.

Donaldson K, Tran L, Jimenez LA, Duffin R, Newby DE, Mills N, et al. 2005. Combustion-derived nanoparticles: a review of their toxicology following inhalation exposure. Part Fibre Toxicol 2:10.

EMEA 2006. Reflection paper on nanotechnology-based medicinal products for human use. European Medicines Agency.

FDA 2007. Nanotechnology Task Force Report 2007. FDA.

Foged C, Brodin B, Frokjaer S & Sundblad A. 2005. Particle size and surface charge affect particle uptake by human dendritic cells in an in vitro model. Int J Pharm 298:315–322.

Gomez S, Gamazo C, Roman BS, Ferrer M, Sanz ML & Irache JM. 2007. Gantrez AN nanoparticles as an adjuvant for oral immunotherapy with allergens. Vaccine 25:5263–5271.

Gomez S, Gamazo C, San Roman B, Ferrer M, Sanz ML, Espuelas S, et al. 2008. Allergen immunotherapy with nanoparticles containing lipopolysaccharide from Brucella ovis. Eur J Pharm Biopharm 70:711–717.

Hellstern D, Schulze K, Schopf B, Petri-Fink A, Steitz B, Kamau S, et al. 2006. Systemic distribution and elimination of plain and with Cy3.5 functionalized poly(vinyl alcohol) coated superparamagnetic maghemite nanoparticles after intra-articular injection in sheep in vivo. J Nanosci Nanotechnol 6:3261–3268.

Holt PG & Stumbles PA. 2000. Characterization of dendritic cell populations in the respiratory tract. J Aerosol Med 13:361–367.

ISO 2008. Nanotechnologies – terminology and definitions for nano-objects – nanoparticle, nanofibre and nanoplate. ISO/TS 27687.

Klippstein R & Pozo D. 2010. Nanotechnology-based manipulation of dendritic cells for enhanced immunotherapy strategies. Nanomedicine.

Lafuse WP, Brown D, Castle L & Zwilling BS. 1995. IFN-gamma increases cathepsin H mRNA levels in mouse macrophages. J Leukoc Biol 57:663–669.

Lah TT, Hawley M, Rock KL & Goldberg AL. 1995. Gamma-interferon causes a selective induction of the lysosomal proteases, cathepsins B and L, in macrophages. FEBS Lett 363:85–89.

Landmark KJ, Dimaggio S, Ward J, Kelly C, Vogt S, Hong S, et al. 2008. Synthesis, characterization, and in vitro testing of superparamagnetic iron oxide nanoparticles targeted using folic Acid-conjugated dendrimers. ACS Nano 2:773–783.

Laurent S, Forge D, Port M, Roch A, Robic C, Vander Elst L, et al. 2008. Magnetic iron oxide nanoparticles: synthesis, stabilization, vectorization, physicochemical characterizations, and biological applications. Chem Rev 108:2064–2110.

Lehmann AD, Parak WJ, Zhang F, Ali Z, Rocker C, Nienhaus GU, et al. 2010. Fluorescent-magnetic hybrid nanoparticles induce a dose-dependent increase in proinflammatory response in lung cells in vitro correlated with intracellular localization. Small 6:753–762.

Mach B, Steimle V, Martinez-Soria E & Reith W. 1996. Regulation of MHC class II genes: lessons from a disease. Annu Rev Immunol 14:301–331.

Manolova V, Flace A, Bauer M, Schwarz K, Saudan P & Bachmann MF. 2008. Nanoparticles target distinct dendritic cell populations according to their size. Eur J Immunol 38:1404–1413.

Maynard AD, Aitken RJ, Butz T, Colvin V, Donaldson K, Oberdorster G, et al. 2006. Safe handling of nanotechnology. Nature 444:267–269.

Montet-Abou K, Daire JL, Hyacinthe JN, Jorge-Costa M, Grosdemange K, Mach F, et al. 2009. In vivo labelling of resting monocytes in the reticuloendothelial system with fluorescent iron oxide nanoparticles prior to injury reveals that they are mobilized to infarcted myocardium. Eur Heart J.

Moss OR & Wong VA. 2006. When nanoparticles get in the way: impact of projected area on in vivo and in vitro macrophage function. Inhal Toxicol 18:711–716.

Oberdorster G, Oberdorster E & Oberdorster J. 2005. Nanotoxicology: an emerging discipline evolving from studies of ultrafine particles. Environ Health Perspect 113:823–839.

Petri-Fink A, Chastellain M, Juillerat-Jeanneret L, Ferrari A & Hofmann H. 2005. Development of functionalized superparamagnetic iron oxide nanoparticles for interaction with human cancer cells. Biomaterials 26:2685–2694.

Petri-Fink A & Hofmann H. 2007. Superparamagnetic iron oxide nanoparticles (SPIONs): from synthesis to in vivo studies – a

summary of the synthesis, characterization, in vitro, and in vivo investigations of SPIONs with particular focus on surface and colloidal properties. IEEE Trans Nanobioscience 6:289–297.

Petri-Fink A, Steitz B, Finka A, Salaklang J & Hofmann H. 2008. Effect of cell media on polymer coated superparamagnetic iron oxide nanoparticles (SPIONs): colloidal stability, cytotoxicity, and cellular uptake studies. Eur J Pharm Biopharm 68:129–137.

Powers M. 2006. Nanomedicine and nano device pipeline surges 68%. NanoBiotech News 1–69.

Regamey N, Obregon C, Ferrari-Lacraz S, Van Leer C, Chanson M, Nicod LP, et al. 2007. Airway Epithelial IL-15 transforms monocytes into dendritic cells. Am J Respir Cell Mol Biol 37:75–84.

Rothen-Rutishauser B, Muhlfeld C, Blank F, Musso C & Gehr P. 2007. Translocation of particles and inflammatory responses after exposure to fine particles and nanoparticles in an epithelial airway model. Part Fibre Toxicol 4:9.

Sallusto F & Lanzavecchia A. 1994. Efficient presentation of soluble antigen by cultured human dendritic cells is maintained by granulocyte/macrophage colony-stimulating factor plus interleukin 4 and downregulated by tumor necrosis factor alpha. J Exp Med 179:1109–1118.

Scholl I, Weissenbock A, Forster-Waldl E, Untersmayr E, Walter F, Willheim M, et al. 2004. Allergen-loaded biodegradable poly(D, L-lactic-co-glycolic) acid nanoparticles down-regulate an ongoing Th2 response in the BALB/c mouse model. Clin Exp Allergy 34:315–321.

Schroder K, Hertzog PJ, Ravasi T & Hume DA. 2004. Interferon-gamma: an overview of signals, mechanisms and functions. J Leukoc Biol 75:163–189.

Steitz B, Salaklang J, Finka A, O'Neil C, Hofmann H & Petri-Fink A. 2007. Fixed bed reactor for solid-phase surface derivatization of superparamagnetic nanoparticles. Bioconjug Chem 18:1684–1690.

Thiele L, Rothen-Rutishauser B, Jilek S, Wunderli-Allenspach H, Merkle HP & Walter E. 2001. Evaluation of particle uptake in human blood monocyte-derived cells in vitro. Does phagocytosis activity of dendritic cells measure up with macrophages? J Control Release 76:59–71.

Trombetta ES, Ebersold M, Garrett W, Pypaert M & Mellman I. 2003. Activation of lysosomal function during dendritic cell maturation. Science 299:1400–1403.

Trombetta ES & Mellman I. 2005. Cell biology of antigen processing in vitro and in vivo. Annu Rev Immunol 23:975–1028.

Tsoli M, Kuhn H, Brandau W, Esche H & Schmid G. 2005. Cellular uptake and toxicity of Au55 clusters. Small 1:841–844.

Von Garnier C, Filgueira L, Wikstrom M, Smith M, Thomas JA, Strickland DH, et al. 2005. Anatomical location determines the distribution and function of dendritic cells and other APCs in the respiratory tract. J Immunol 175:1609–1618.

Von Garnier C & Nicod LP. 2009. Immunology taught by lung dendritic cells. Swiss Med Wkly 139:186–192.

Von Garnier C, Wikstrom ME, Zosky G, Turner DJ, Sly PD, Smith M, et al. 2007. Allergic airways disease develops after an increase in allergen capture and processing in the airway mucosa. J Immunol 179:5748–5759.

Von Zur C, Von Elverfeldt D, Bassler N, Neudorfer I, Steitz B, Petri-FInk A, et al. 2007. Superparamagnetic iron oxide binding and uptake as imaged by magnetic resonance is mediated by the integrin receptor Mac-1 (CD11b/CD18): implications on imaging of atherosclerotic plaques. Atherosclerosis 193:102–111.

Warheit DB, Webb TR, Colvin VL, Reed KL & Sayes CM. 2007. Pulmonary bioassay studies with nanoscale and fine-quartz particles in rats: toxicity is not dependent upon particle size but on surface characteristics. Toxicol Sci 95:270–280.

Wegmann KW, Wagner CR, Whitham RH & Hinrichs DJ. 2008. Synthetic Peptide dendrimers block the development and expression of experimental allergic encephalomyelitis. J Immunol 181:3301–3309.

Wikstrom ME, Batanero E, Smith M, Thomas JA, Von Garnier C, Holt PG, et al. 2006. Influence of mucosal adjuvants on antigen passage and CD4+ T cell activation during the primary response to airborne allergen. J Immunol 177:913–924.

Wolf PR & Ploegh HL. 1995. How MHC class II molecules acquire peptide cargo: biosynthesis and trafficking through the endocytic pathway. Annu Rev Cell Dev Biol 11:267–306.

Xia T, Kovochich M, Brant J, Hotze M, Sempf J, Oberley T, et al. 2006. Comparison of the abilities of ambient and manufactured nanoparticles to induce cellular toxicity according to an oxidative stress paradigm. Nano Lett 6:1794–1807.

Yang D, Zhao Y, Guo H, Li Y, Tewary P, Xing G, et al. 2010. [Gd@C(82)(OH)(22)](n) nanoparticles induce dendritic cell maturation and activate Th1 immune responses. ACS Nano 4:1178–1186.